*Journal of the European Ceramic Society* **18** (1998) 1743–1752

PII: S0955-2219(98)00009-0
0955-2219/98/$—see front matter

# Alumina–Chromium Cermets by Hot-Pressing of Nanocomposite Powders

J. L. Guichard, O. Tillement and A. Mocellin*

LSG2M, U.R.A. 159, Ecole des Mines, Parc de Saurupt, 54042 Nancy Cedex, France

(Received 22 September 1997; accepted 19 December 1997)

***Abstract***

*Alumina–chromium cermets with up to 36 vol% metal have been prepared from powders obtained by high energy ball-milling. Firstly, the powder is prepared from initially blending $Cr_2O_3$ or $CrO_3$ and Al for reactive milling and from $Al_2O_3$ and Cr for a direct milling. The materials as-pressed at 1400°C under 30 MPa consist of an alumina based matrix with metallic Cr inclusions. The difference of reactivities between $Cr_2O_3$ and $CrO_3$ during milling on the final material is discussed and the advantages of reactive compared to direct milling are emphasised. In a second part, the more efficient technique is used to obtain cermets with different compositions. Nanostructured powders were synthesized from $Cr_2O_3$, Al and $Al_2O_3$. The influence of chromium metal content is studied by microstructural observations, physical, mechanical and electrical properties evaluations. The expected improvement of mechanical properties compared to pure alumina is indeed observed. The importance of the milling time and the temperature–pressure cycle during the forming and sintering process are reflected on the final material structure and properties.* © *1998 Elsevier Science Limited. All rights reserved*

## 1 Introduction

The application of ceramics as structural components is often limited by their brittleness. The addition of second phase inclusions which influence the propagation of cracks and the choice of ductile materials for reinforcing the matrix have been one much studied approach to overcome such a drawback.

The first metallic dispersions used in alumina were chromium particles.[1,2] Since these studies, several other metals have been associated with alumina.[3–5] In fact, the alumina chromium combination indeed appears an appealing one. Aluminium and chromium oxides have the same crystal structure and are completely soluble into each other[6] which may be favourable for the achievement of good bonding between the metal and oxide phases. However despite very close thermal expansion coefficients [respectively, $6\times10^{-6}\,°C^{-1}$ (Ref. 7) and $6{\cdot}2\times10^{-6}\,°C^{-1}$ (Ref. 8) for alumina and chromium], excellent oxidation resistance and chemical stability provided by alumina and chromium, these composites so far have had a poor thermal shock resistance and a weak fracture toughness.

Since the 1950s, several processing routes have been considered. The powder preparation can be a simple gentle ball milling of ceramic and metal powders in order to minimize temperature rising, oxidation and particles coagulation.[2,9,10] The slurry is dried and the mixture is formed and sintered by conventional powder metallurgical techniques. Reactive sintering is also an interesting way to produce a wide range of ceramic–metal composites. Such synthesis of ceramic–metal composites by reaction between aluminium and various oxides has been achieved.[3,11]

More recently, Tuan *et al.*[12] obtained alumina–metal composites from initial powder mixtures such as alumina and nickel oxide. The powder was formed and during the sintering under reducing atmosphere, the nickel oxide was reduced to nickel. The size of nickel inclusions is thus limited by the size of NiO particles. Also, in order to prepare $Al_2O_3$–Ni composites with smaller inclusions, a nickel coating was achieved by impregnating alumina powder in a nickel nitrate solution.[13] The dried powder was reduced in a hydrogen atmosphere at 500°C for 12 h to obtain nanometer size nickel deposited on alumina particles. Devaux[5] has prepared $Al_2O_3$–Fe and $Al_2O_3$–$Fe_{0.8}Cr_{0.2}$

*To whom correspondence should be addressed.

nanocomposites by chemical synthesis. The coprecipitation of metal oxalates gives rise after decomposition to homogeneous and well dispersed oxide solid solutions. The hydrogen reduction of these solid solutions leads to a stable dispersion of nanometric metal particles within the grains of a powdered ceramic matrix.

The sol–gel technique could be advantageous for metal–ceramic composite powders preparation because of its potential to achieve fine-scale homogeneity. Breval *et al.*[14] have tried to make monolithic ceramic–metal composites ($Al_2O_3$–Ni) with a well-dispersed metal phase from 10 up to 50 wt%. In their case, the gel was prepared using an alkoxide precursor, then was dried. Before forming the nickel oxide is converted to metal with a treatment for 4 h at about 1000°C in $H_2$. However the relatively high cost of some reactants, the limitation of the metallic oxide to reduce and the difficulty to control the gel drying step are drawbacks of this method. Several researches focus on Al–$Al_2O_3$ obtained by direct metal oxidation or reactive melt penetration.[15] But the low melting point of Al leads to limitations of the practicable service temperatures. Thus, more refractory metals or intermetallics should be used as reinforcing phase[16] but they imply complicated and more expensive processing techniques like HIP, hot-extrusion or gas-pressure metal infiltration. Recently Claussen *et al.*[17] prepared $Al_2O_3$–aluminide alloys (3A) and $Al_2O_3$–Al alloyed metal composites (3AMC). Oxidation and reduction reactions occur at the grain surfaces to yield $Al_2O_3$ composites containing aluminides and/or metals, respectively.

Besides all these classical or more recent ways for composite powder or bulk synthesis, mechanical alloying appears as a powerful technique.[18] Direct milling ($Al_2O_3 + Cr$) yields simple mechanical homogeneization by crystallites size reduction whereas with an initial powder mixture of aluminium and metal oxide, alumina based composites are obtained by a displacement reaction induced by reactive ball-milling,[19] which is basically analogous to a controlled conventional thermite reaction. The obtained micronic powders are made of homogeneous nanoscaled crystallites dispersion and the reactivity of the product can be controlled.[20]

The physical and chemical stabilities of the reactant oxides have important effects on the ignability of thermite mixtures.[21] For Chernenko *et al.*,[22] $Cr_2O_3$ falls under oxides of class 1 which are chemically and physically stable. This oxide is inert up to the moment of ignition. When such thermite reaction is carried out in air, the oxidation of aluminium by atmospheric oxygen initiates the combustion of the mixture. In our case, the following reaction takes place during milling at room temperature:[19]

$$2Al + Cr_2O_3 \rightarrow Al_2O_3 + 2Cr$$
$$\Delta H_r = -535 \text{ kJ mol}^{-1}$$

$CrO_3$ in turn falls in the case of class 3 oxides which are chemically unstable. The ignition process is more complex because oxygen liberated by the decomposition of the oxide can play a significant role in developing the combustion reaction. For example, the ignition of the $CrO_3$–Al mixture can occur at as low a temperature as about 170°C, which is the decomposition temperature of $CrO_3$:[22]

$$2Al + CrO_3 \rightarrow Al_2O_3 + Cr$$
$$\Delta H_r = -1080 \text{ kJ mol}^{-1}$$

The heat of reaction is much higher ($-1080\,\text{kJ mol}^{-1}$ against $-535\,\text{kJ mol}^{-1}$), so the reaction occurs more rapidly and the milling time can be decreased. On the one hand, with a decreased milling time, the contamination which comes from the grinding media should be reduced but on an other hand, the reaction is much more violent and could damage the grinding steel media more rapidly. The main advantage using this latter oxide is to obtain with still a stoechiometric reaction ($CrO_3 + 2Al$) a composite powder with a reduced metal content (21 vol%) against 36 vol% for the reaction with ($Cr_2O_3 + 2Al$).

The aims of this work are firstly to compare the reactive and the direct (i.e. non reactive $Al_2O_3 + Cr$) milling ways, secondly to evidence the influence of the reactivities of different oxides for the same system, thirdly to optimise the milling time and the temperature–pressure cycle and finally to characterize materials with the different $Al_2O_3$–Cr compositions so obtained.

## 2 Experimental Procedures

### 2.1 Sample preparation

The starting powders were commercially available aluminium (Ecka AS 011), alumina (Martinswerk HRA-5), chromium oxides ($Cr_2O_3$: Riedel de Haen, $CrO_3$: Labosi) and chromium metal (Cerac). Average particle sizes of these powders were in the micrometer range except for chromium ($\approx 100\,\mu m$). The as-received atomized aluminium was oxidized on its surface and the typical alumina content was 0·5–1 wt%.

In order to obtain composites with about 22 vol% Cr, the first reactions investigated which take place during ball-milling are as follows:

$$Al + 0{\cdot}5Cr_2O_3 + 0{\cdot}5Al_2O_3 \rightarrow Al_2O_3 + Cr2$$
$$Al + CrO_3 \rightarrow Al_2O_3 + Cr$$

And in order to compare reactive and direct milling, composite powder was obtained from alumina and chromium metal blended in equimolar amounts.

In the second part of this work, composites with different compositions were synthesized according to the following displacement reaction:

$$2xAl + xCr_2O_3 + (1 - x)Al_2O_3 \rightarrow Al_2O_3 + 2xCr$$

The contents of chromium in the final composition have been chosen in the range of $x = 0$ to $x = 1$ which is the stoechiometric composition of the oxydo-reduction reaction. This corresponds to a volume fraction of metallic phase of 0–36%. For this study, three different compositions have been chosen with 9, 22 and 36 vol% Cr.

For the stocchiometric composition (36 vol% Cr), different milling times were chosen in order to observe the influence of the mechanical activation on the final dense materials. So powder blends were milled during 5 min, 1, 2 and 4 h with the other milling conditions mentioned below.

High energy milling was carried out in a planetary ball-mill (Fritsch Pulverisette 5) under argon atmosphere. Grinding utensils (15 balls of 20 mm diameter and vials) were hardened chromium steel. Stoechiometric mixtures of $Cr_2O_3$ and Al with the adjusted excess alumina have been milled during 4 h with a powder-to-ball mass ratio of 1 to 20, as revealed to be the optimised ratio for this system.[23] The same ratio is kept for the other millings with 2 h for ($CrO_3$ + Al) blend and 4 h for ($Al_2O_3$ + Cr) mixture. As identified on the XRD patterns, $\alpha$-$Al_2O_3$ and Cr were the only two crystalline phases to be found in the as-milled powders. Figure 1 shows the morphology and the microstructure of typical mechanosynthesized powder particles. After such high reactive milling, nanometer sized cristallites are produced from the initial micrometer sized powders. The particles consist of finely divided aggregates of cristallites 20–30 nm in size with presumably an extremely high defect density due to the mechanical action[24] and the powder nanostructure.[25] The mean crystallite size, as estimated by X-ray line broadening[26] lies around 10 nm for both the ceramic and the metallic phases. The corresponding particles appear as a very fine-scale homogeneous assemblage of $\alpha$-alumina and chromium.

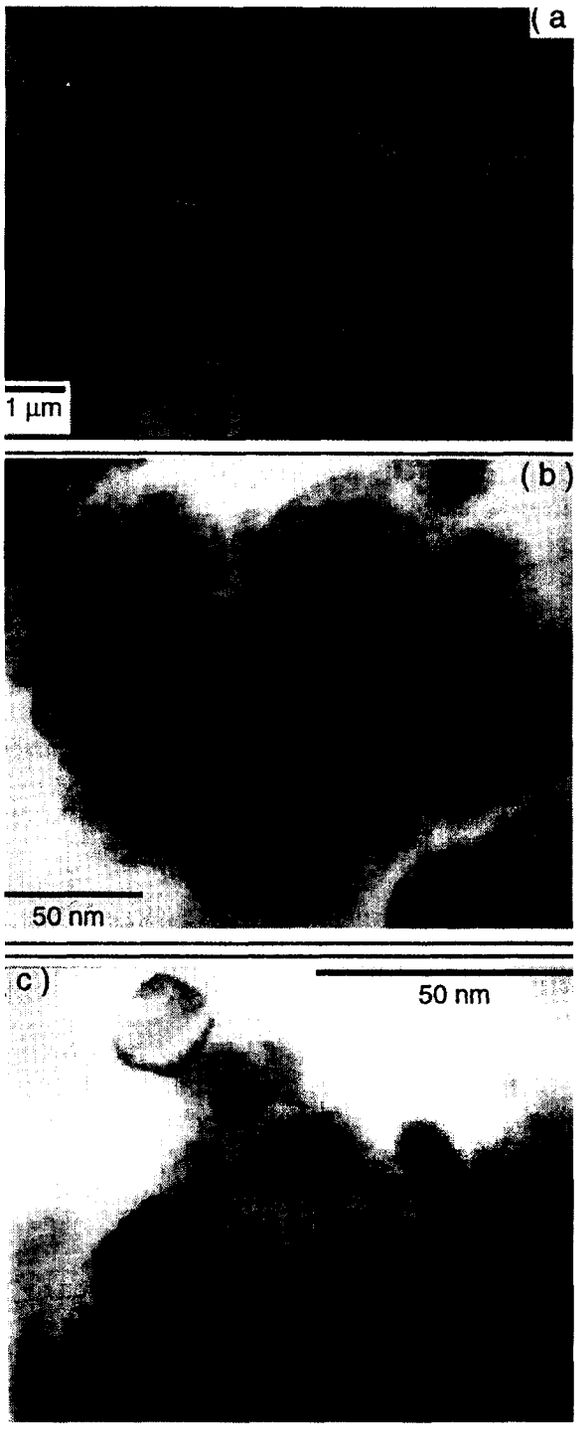


**Fig. 1.** (a) SEM and (b, c) TEM photographs of the stoechiometric Al + $Cr_2O_3$ powder after 4 h reactive milling.

Due to particle welding during high energy milling, some relatively large agglomerates have been formed ($\approx 20\,\mu$m diameter). Therefore, the powders were subsequently wet-ground in Tetrahydrofuran for 2 h. The resulting slurry was dried with a rotary evaporator. The mean particle size is reduced to about 5 $\mu$m after dispersion in propanol-2 with ultrasonics. Then the powder was hot-pressed in a graphite die. Heating under vacuum

was conducted up to 1400°C. The selected sintering cycle was an initial pressureless heating up to 800°C (10°C min$^{-1}$) followed by heating under a constant 30 MPa applied pressure to 1400°C (30°C min$^{-1}$) with a hold time of 30 min at this temperature. The details of load and temperature profiles during hot-pressing are shown in Fig. 2 The measurements of the distance between the pistons, by means of linear voltage displacement transducer (LVDT) positioned inside the vacuum chamber, are related to the relative densities evolution and can be used to study the sintering kinetic.

### 2.2 Characterisation of samples

Density measurements using Archimedes' principle were made on the as-sintered samples which also were prepared for microstructural and mechanical characterisation using standard techniques. From the as-pressed discs (5 mm × Φ 30 mm), dense bars were cut; the dimensions were about 3 mm (height), 4 mm (width) and 25 mm (length). The machining damage was removed mechanically by polishing, ultimately with 1 $\mu$m diamond paste to produce an optical finish. The edges were chamfered to avoid surface defects located at a specimen edge.

The microstructures were studied by high-magnification optical microscopy (Reichert–Jung), and scanning electron microscopy (SEM) (Jeol JSM 6400F). The surfaces were coated with gold to avoid charging during SEM observations. No etching was necessary to outline morphological aspects of chromium dispersions. The contrast between both phases was sufficient to obtain good micrographs. Composite microstructures were quantitatively analysed (porosity and metallic particle size and morphology) by Visilog image processing (Noesis Vision).

Rupture strength measurements were made with a Zwick machine (model 1446) using the four-point bending mode with an inner and outer span of 10 and 20 mm, respectively, and a displacement rate of 0·1 mm min$^{-1}$. Average values are calculated from three tests.

Hardness (HV10) was obtained with a Vickers diamond indenter using 98 N load and a loading rate of 10 N s$^{-1}$. The diagonal of the obtained indentations was much larger (> 100 $\mu$m) than the scale of microstructure. The accuracy of the measurements was ±0·5 GPa. Fracture toughness was estimated by the indentation strength technique.[27] The impression was made on faces parallel to the hot-pressing axis. Beams were then fractured in the four-point bend test with a displacement rate of 0·1 mm min$^{-1}$. Crack profiles have been checked (by optical microscopy) prior to testing and it is assumed that rupture did take place from those microcracks induced by indents. With a high metal content, the materials exhibit lightly plastic fracture behaviours, and more refined analyses evidently would be desirable but are beyond the scope of the present work. Thus, from the fracture strength, $\sigma f$, and the indent load, $P$, the fracture toughness is calculated by eqn (1):[27]

$$K_c = \eta(E/H)^{1/8}(\sigma_f.P^{1/3})^{3/4} \quad (1)$$

where $E$ is Young's modulus, $H$ is the hardness and $\eta$ is a geometrical constant for which a value of 0·59 was used, as suggested in the literature.[27]

The Young and shear moduli were measured using the ultrasonic transmission method (transductor Panametrics and pulser receiver model 5052 PRX Panametrics).

The room-temperature electrical conductivity of our samples was measured using a four-probe method with separate voltage and current electrodes. Several resistance measurements were performed for each sample by choosing different points on the sample as voltage contacts, and the final resistance of each sample was determined by averaging the measured values. The current-voltage characteristics of all the samples were linear (Ohmic) in our measurement conditions.

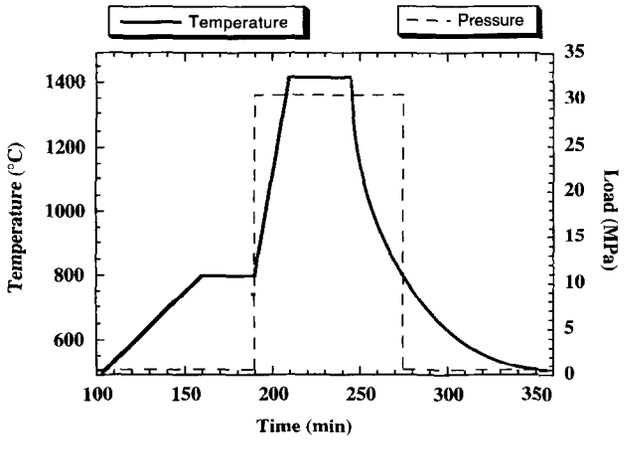


Fig. 2. Temperature and pressure cycle during hot pressing.

## 3 Results and Discussion

### 3.1 Comparison between reactive and direct millings ($Al + Cr_2O_3$, $Al + CrO_3$ and $Al_2O_3 + Cr$)

In Fig. 3, optical micrographs of $Al_2O_3 - Cr$ (22 vol%) dense composites obtained from $(Al + Cr_2O_3)$, $(Al + CrO_3)$and$(Al_2O_3 + Cr)$ are presented. The first two which result from reactively milled powders are more homogeneous: the metal inclusion distribution is more regular. In fact the sample densified with powder from direct

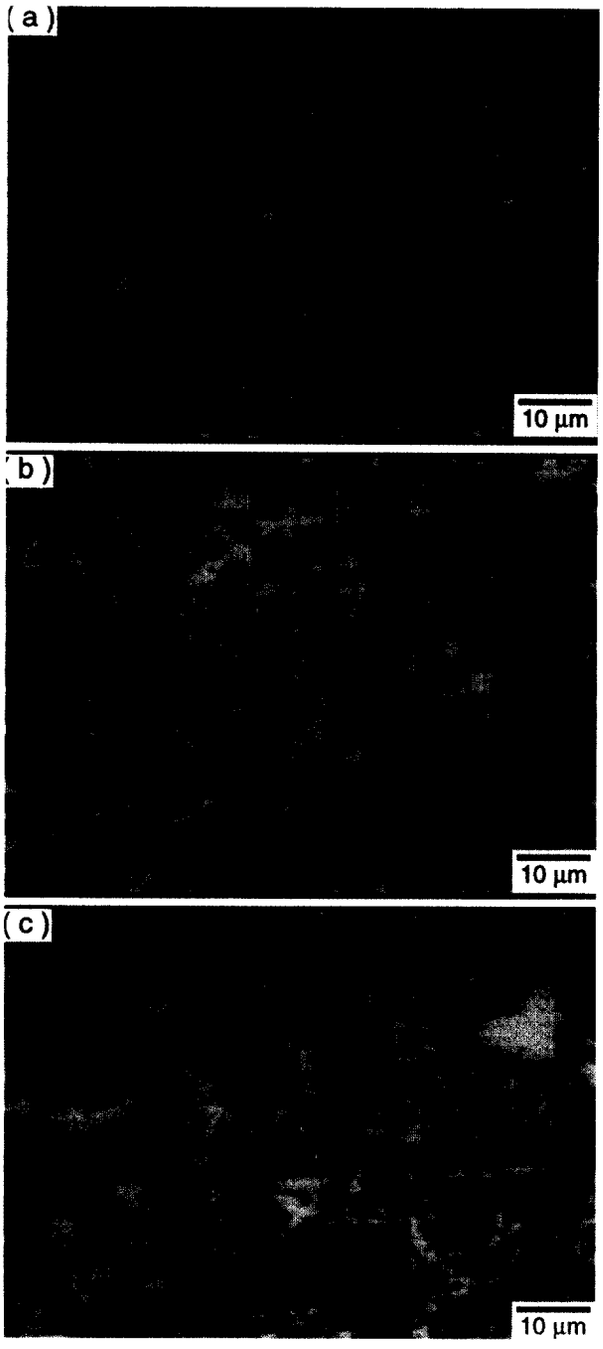


**Fig. 3.** Optical micrographs of alumina–22 vol% Cr obtained from (a) $Al + Cr_2O_3$; (b) $Al + CrO_3$; and (c) $Al_2O_3 + Cr$.

milling has a microstructure with widely varying metal inclusion sizes.

Figure 4 shows the size distributions for the three materials the metal inclusion sizes and shapes which characterize the particles morphology.

All the three composites have more than a half their metal inclusion numbers with submicrometer sizes (89, 76 and 70% for composite obtained from, respectively, $Al + Cr_2O_3$, $Al_2O_3 + Cr$ and $Al + CrO_3$). The inclusion mean surface area can be used to compare the samples. Only the material prepared from initially Al and $Cr_2O_3$ has a mean surface area below 1 square micrometer (0·54) compared to the others (1·06 and 1·29) The standard deviation (respectively, of 0·26, 0·53 and 0·62) on this value can characterize the size homogeneity. Among these composites, the first one (from $Al + Cr_2O_3$) is the more regular and homogeneous. The others have important standard deviations of their mean surfaces. These differences are believed to be related to the more energetic reaction for the ($Al + CrO_3$) sample which leads to bigger metal inclusions or for the direct milling to the initial ductile metal particles flatening. In order to characterize the dispersion of the chromium inclusions, the mean free path in the ceramic matrix can also be measured. As for the inclusions mean sizes, these values [2·70 $\mu$m for ($Al + Cr_2O_3$), 3·75 $\mu$m for ($Al + CrO_3$) and 4·20 $\mu$m for ($Al_2O_3 + Cr$)] confirm the better homogeneity of the first composite compared to the others.

The quantitative image analyses, which slightly underrate the metal content, show that the metallic phase amount is higher for direct and ($Al + CrO_3$) reactively milled composites ($\geq$20·5 vol% for $Al + Cr_2O_3$ compared to $\geq$22 vol% for the other two). The pollution is higher for direct than reactive milling. The difference in the metal content is essentially due to contamination by the grinding media as shown by Osso[23] on the basis of Mössbauer spectroscopy. In the direct milling case, abrasive alumina is initially in high amount whereas it is the heat of reaction for ($Al + CrO_3$) which may have affected the surface properties of the grinding media.

All samples have a hardness value between 15 and 16 GPa because of their similar metal contents. No difference arising from the initial powder mixtures is noticed.

It follows from these observations that reactive milling yields materials with homogeneous microstructures, and better controlled final chemical composition with less contamination. Also, in practice, the synthesis of composites from ($Al + Cr_2O_3$) is easier in spite of a longer grinding

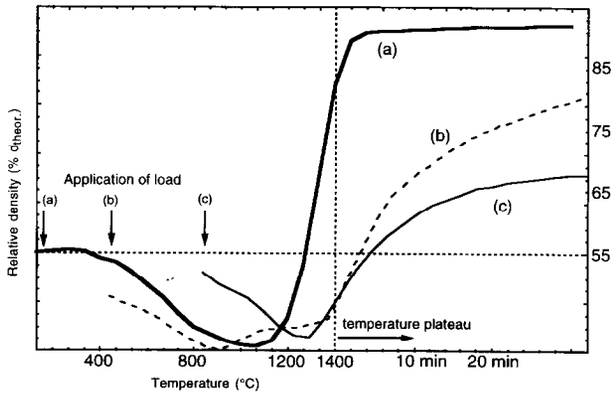


**Fig. 4.** Inclusion size distribution for the three materials presented in Fig. 3.

time (4 h) due to the more progressive reduction of chromia. The reaction can be monitored and a simple mechanical activation during milling is also possible. In this latter case, the powder blends which come from the mill are subsequently more reactive and a moderate thermal treatment allows to achieve the reduction.

Different milling times will give powders with different reactivities, and consequently different sintering kinetics and then various microstructures in the consolidated materials, as will be illustrated below.

The $CrO_3$ utilization leads to a violent reaction which impedes chemical homogeneization whereas, from $(Al + Cr_2O_3)$, a more progressive reaction, powders exhibit a composite structure with homogeneous distribution of metal and ceramic phases in the nanometer ranges.

### 3.2 Consolidation of reactively milled $(Al + Cr_2O_3)$ powders

*3.2.1 Influence of metal volume fraction*

The obtained samples are homogeneous. Radial and longitudinal profiles of the metal phase amount have been obtained from several pellets. There is no metal concentration gradient between the surface and the core of the pellets and the metal content is almost the same everywhere. Globally, when the metal amount increases, the metallic inclusions size increases and their morphology becomes more interpenetrating with ramifications as shown on Fig. 5. The particles with such shape seem to be firmly bonded to the ceramic matrix. We can notice porosities which come mainly from metal/ceramic interface decohesion due to a metal globularization beginning, from powder behaviour during forming and also from metallographic preparation leading to grains pulling out.

The conductivities of the different composites have been measured to characterize the chromium metal distribution. For ideal metal/insulator composites and above a critical metallic volume fraction ($x_c$) also known as the percolation threshold, the effective conductivity of the composite $\sigma_{eff}$ can be expressed in the form:

$$\sigma_{eff} = \sigma_o(x - x_c)^t \text{ for } x > x_c$$

where $\sigma_o$ is the conductivity of the metallic phase and $t$ the conductivity exponent.[28] Amongst the various parameters that influence the percolation threshold and the conductivity exponent, the most important factors are the metal distribution, the metal shape and the metal-ceramic interactions. No definite transition from insulating to metallic

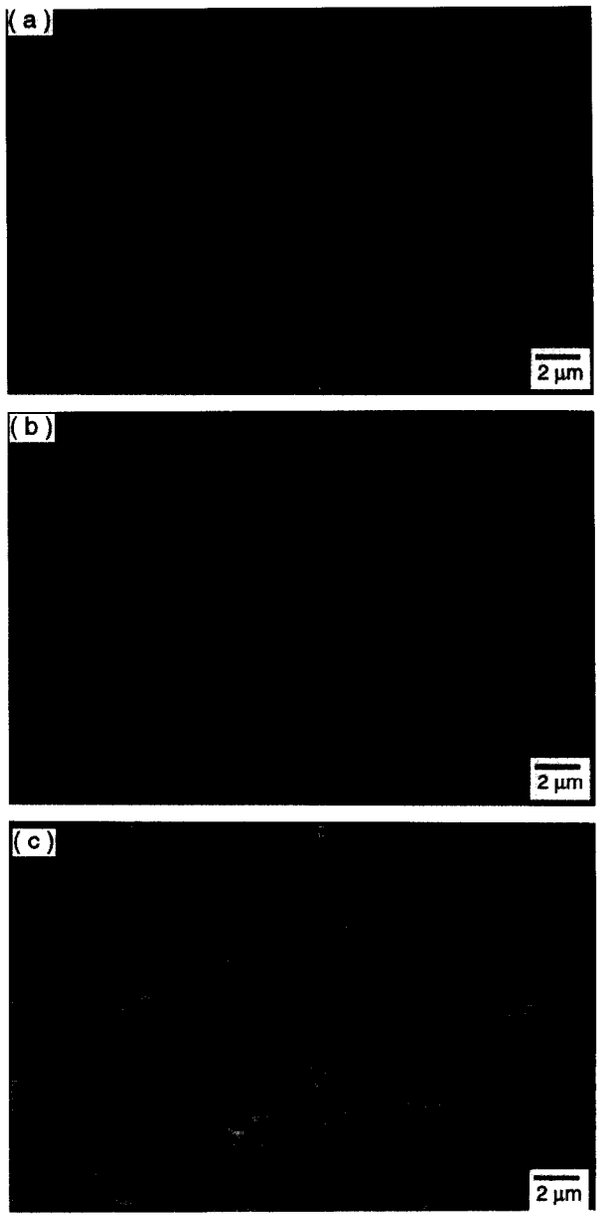


Fig. 5. SEM micrographs for different compositions obtained from $Al + Cr_2O_3 + xAl_2O_3$: (a) 9 vol%, (b) 22 vol% and (c) 36 vol% Cr.

behaviour is observed in the present set of samples. The percolation concentration ($x_c$) can therefore be estimated to be about 6–7 vol% Cr[28] and the conductivity exponent to reach $6 \pm 0{\cdot}2$. This value is much higher than for $Al_2O_3$–Fe[4] (respectively, 19% and 3·2). Such a high value of the critical exponent can be attributed to the complex microstructure of metallic particles and the existence of narrow necks in the conducting paths with multiple contacts between adjacent particles. This difference is believed due to a better ceramic/metal interface and the more interwoven microstructure,[29] confirmed by the SEM micrographs (Fig. 5).

As expected, the hardness decreases as the metal content increases. It varies from about 20 GPa for pure alumina to 12 GPa for the stoechiometric composite with 36 vol% Cr. This latter value is

higher than the one obtained for a similar alumina–36 vol% Fe (6·5 GPa).[4] This important difference of hardness for composites with similar metal contents may not only be due to the different nature of the metal but to the solution of some chromia $Cr_2O_3$ in the alumina matrix[30] and to a better coherency at the interface too. Both oxides have the same crystal structure and are completely soluble into each other. Shinozaki *et al.*[29] showed that the solution of 20 atom% of $Cr_2O_3$ in $Al_2O_3$ can increase the matrix hardness from 20 to 24 GPa. In our samples, chemical measuring out leads to a $Cr_2O_3$ content superior bound of about 10% atomic.

The results of the mechanical properties tests show that the fracture toughness increases from 4 to 7·2 MPa $m^{1/2}$ as the metal content varies from 9 to 36 vol% Cr. This reinforcement is likely due to interface decohesion and, for the bigger inclusions, to some plastic deformation (cf. Figure 6).[4] In order to go on its propagation, the crack has to stretch the metallic inclusions (energy is then dissipated by plastic deformation) or to bypass the ductile particles (energy so is used to create a higher new surface area). In these two cases, the crack is slowed down and fracture toughness is increased. The Young and shear moduli decrease as expected from, respectively, 400 and 160 GPa for pure alumina to 340 and 135 GPa for the stoichiometric composition.

As reported in Table 1, the rupture strength is maximal for the 22 vol% Cr composite with 550 MPa. These measurements must be considered to only represent order of magnitude figures because of imprecise statistics as well residual porosity effects.

Whatever the metal content is, the samples have a good interface cohesion between ceramic and metal phases. The low percolation threshold can be explained by the chromium homogeneous filamentous microstructure due to the nanoscaled mechanosynthesized powders.

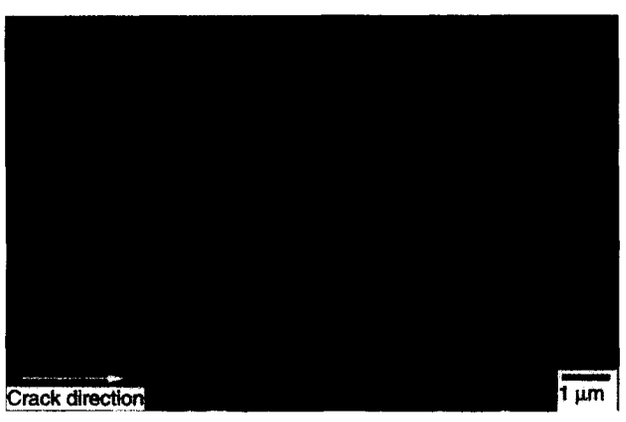


**Fig. 6.** Interactions between cracks and metal inclusions ($Al_2O_3$–Cr 22 vol% Cr).

*3.2.2 Powders reactivity modification*

For one composition (36 vol% Cr), powder blends were milled for varying lengths of time: 5 min, 1, 2 and 4 h in steel vials.

After 5 min milling, the chromia reduction has not yet begun. The powders have been only mixed. The DTA curve, in Fig. 7, shows the behaviour of this blend during subsequent heat treatment. The endothermic pic corresponds to aluminium melting (660°C) and the high exotherm at 1100°C is the oxydo-reduction reaction.[20] Chromia is reduced in a simple direct but progressive way according to the following thermal displacement reaction as expected:

$$Cr_2O_3 + 2Al_{(liq)} \rightarrow \alpha\text{-}Al_2O_3 + 2Cr$$

As the milling time increases, the endothermic pic disappears and the exotherm takes place at lower temperatures with smaller intensities. So, for 1 and 2 h, the reaction has been activated mechanically and will be effected by thermal treatment.

The DTA curve for the 4 h milled powder does not exhibit any variation. The reaction takes place essentially during milling.

After uniaxial hot-pressing, under the same forming conditions as previously (Fig. 2), these powders with different reactivities lead to different microstructures (Fig. 7). Materials obtained from 5 min and 4 h milled powders have a high density (> 95% $d_{th}$) whereas the reactive powder (milled 2 h) yields lower densities, about 70%. In this case the metal inclusions are bigger and more spherical.

So, powders with different reactivities can be elaborated and adapted in order to obtain the expected bulk microstructure.

**Table 1.** Properties of the various $Al_2O_3$–Cr compositions

| *Composition* | *Density* ($g\,cm^{-3}$) | *Relative density* (%) | *Hardness* (GPa) | *Fracture strength* (MPa) | *Fracture toughness* ($MPa\,m^{1/2}$) | *Electrical conductivity* ($S\,cm^{-1}$) |
|---|---|---|---|---|---|---|
| $Al_2O_3$ + 0% Cr | 3·88 | 97·5 | 21·2 | 350 | 3 | $10^{-13}$ |
| + 9% Cr | 4·27 | 97·8 | 17·5 | 380 | 3·2 | $2{\cdot}5\ 10^{-2}$ |
| + 22% Cr | 4·55 | 97·0 | 16·5 | 550 | 4·3 | 13 |
| + 36% Cr | 5·10 | 99·2 | 12·3 | 440 | 7·2 | 729 |
| $Al_2O_3$/Cr from Al + $CrO_3$ | 4·58 | 97·4 | 15·5 | — | 7 | 141 |

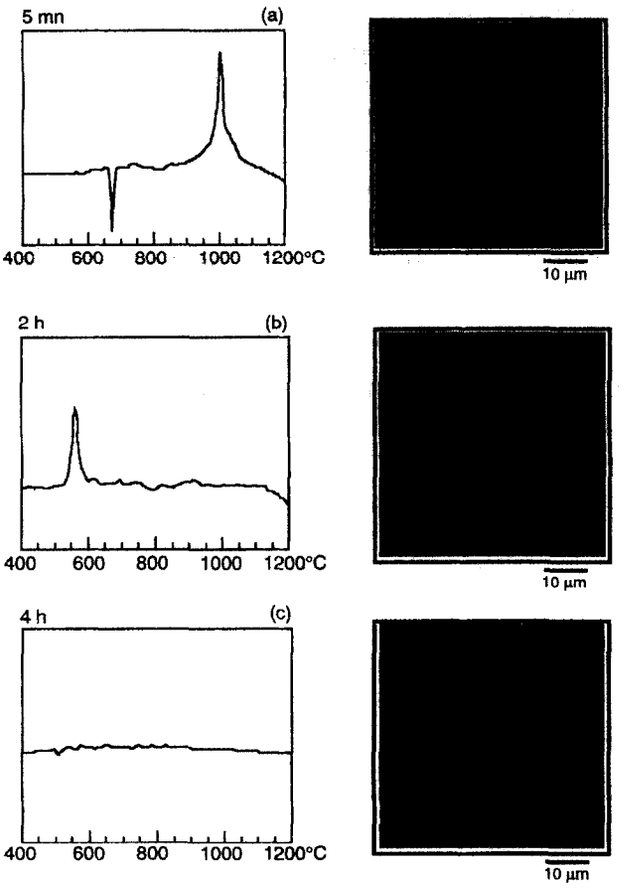


**Fig. 7.** DTA curves for different time milled powders ($Al + Cr_2O_3$) and microstructures of correspondant sintered materials: (a) 5 min, (b) 2 h and (c) 4 h.

### *3.2.3 Influence of forming and sintering for a homogeneous reactive powder*

A stoechiometric composition milled 2 h is densified with three different pressure/temperature cycles. We have seen that when the pressure is applied at 800°C, the obtained material is very porous with big and globular metal inclusions. After a 2 h mill, the reaction of reduction takes place at 550–600°C as visible on the DTA curve (Fig. 7). So for this experiment, the reaction occurs before pressure is applied and it is conceivable that the corresponding heat released will cause some local melting.

In a second experiment, the pressure is applied 300°C below on the same powder (2 h milled). The as-pressed pellet is more dense (about 82% theoretical density) but still inhomogeneous in the metal inclusion size.

Finally with the pressure applied at ambient temperature, the reaction takes place under pressure and the material is dense (> 95% $d_{th}$) and much more homogeneous than the two previous ones. The obtained microstructure is finer and similar in inclusion size to the composites presented in Fig. 7(a) and (c).

The three shrinkage curves (cf. Fig. 8) which characterise also the sintering of these samples present a volume increase between 450 and 1100°C. Munir[31] suggests four different reasons for porosities and volume increases in products of combustion synthesis: changes in the molar volume during the reaction, gas evolution due to volatile impurity expulsion, thermal migration resulting from high thermal gradients and existing porosity in the reactants. Among these four hypothesis, only gas emission and important migration and rearrangements resulting from high thermal gradient can a priori explain the initial volume increase before sintering. Moreover, the reaction is very exothermal (the adiabatic temperature is about 2110°C) and may cause eventually state or phases changes.[32]

The gas emission hypothesis is not likely:no weight loss was noticed during thermogravimetric experiment. But the TGA sample and pellet obtained with load application after 800°C show enormous globular metal particles. This inclusion morphology results from metallic phase melting, which is confirmed by the XRD pattern to be chromium metal. This behaviour seems dependent on the rate of temperature increase and is observed only for a high one ($\approx 30°C\,min^{-1}$). Locally, during the oxydoreduction process, the temperature rise may be very important, sufficient to reach the Cr melting point (> 1875°C). Because of the important difference between liquid and solid chromium density (respectively, 6·3[33] at melting temperature and 7·2 at ambient temperature), the volume variation which occurs during the phase change is about 13–14% and thus is of the right order to account for the volume increase observed in the three samples and estimated about 15–17%. With the presence of a transient liquid phase, the separation between the two phases (ceramic and metal) may be more effective and allows to explain the obtained microstructure for the sample when pressure is applied at 800°C.

As showed by Dunmead *et al.*,[34] by applying mechanical pressure during the combustion reaction leading to TiC/Ni–Al composites, products

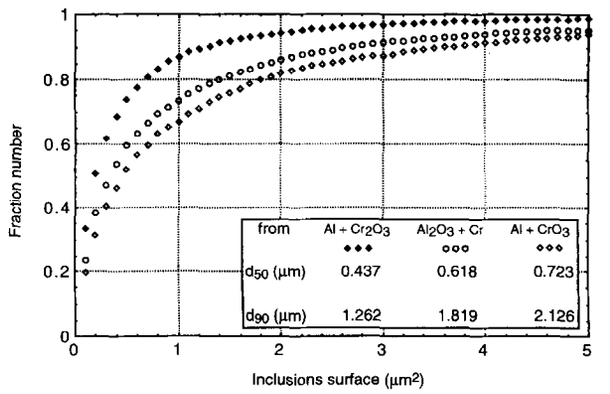


**Fig. 8.** Sintering curves. $Al + Cr_2O_3$ milled 2 h powders are consolidated up to 1400°C under 30 MPa during 30 min. The temperature of pressure application is (a) ambient, (b) 450°C and (c) 800°C.

with important relative density were obtained. In our case, the reaction and the rearrangement caused by the local Cr melting are constrained by the applied pressure, the Cr solidification occurs during composite sintering, yielding more dense materials with homogeneous microstructure. Moreover, the energy produced by the reaction may be drained off more rapidly when the charge is loaded. The temperature increase so should be more moderate. We observe such phenomena for the ($Al + Cr_2O_3$) 2 h milled powder when the load is applied at ambient temperature, quite similarly to what Dunmead *et al.*[34] have reported.

## 4 Conclusion

Ceramic-metal composites in the alumina–chromium system have been prepared from three differently synthesized powders, i.e. with direct $Al_2O_3$ and Cr, and with reaction between $Cr_2O_3$ and Al, between $CrO_3$ and Al in a high energy ball mill. The progressive reduction of $Cr_2O_3$ seems to be easier to control and monitor. So this approach was further investigated and the influence of different parameters was studied: the metallic phase amount (9 up to 36 vol% Cr), the milling time for the stoechiometric composition and the consolidation temperature/pressure cycle.

Notable results include the reinforcement of the matrix due to the metal inclusions. Different milling times yield powders with different reactivities and consequently, materials with different densities, microstructures and properties. Finally, for a given powder, the temperature at which pressure is applied during the consolidation cycle has a profound influence on the final density and homogeneity of microstructure. The ability to control the size and the morphology of the reinforcing phase gives thermal displacement reaction processing by mechanosynthesis important advantages over other routes.

## References


1. Tinklepaugh J. R. and Crandall, W. B., *Cermets*, Reinhold, New York, 1960,
2. Shelvin, T. S., Fundamental study and equipment for sintering and testing of cermets bodies: IV. Fabrication, testing and properties of 72 chromium–28 alumina cermets. *J. Am. Ceram. Soc.*, 1954, **37**, 140–1453.
3. Osso, D., Mocellin, A., Le Caer, G. and Pianelli, A., Preparation of alumina–chromium composites by reactive hot-pressing $Al + Cr_2O_3$ based powders. *J. de Physique IV, Colloque C7*, 1993, **3**, 1311–1316.
4. Guichard, J. L., Tillement, O. and Mocellin, A., Preparation and characterization of alumina–iron cermets by hot-pressing of nanocomposites powders. *J. Mat. Sci.*, 1997, **32**, 4513–215.
5. Devaux, X., Nanocomposites à matrice céramique: systèmes alumine–métaux de transition (fer, chrome) et alumine–alliages fer–chrome, Ph.D. thesis, Université Paul Sabatier, Toulouse, France, 1991.
6. Bunting, E. N., *Bur. Stand. J. Res.*, 1931, **6**, 948.
7. Beadless, R. L., Handbook of tables for applied engineering science, Ed. R. C. Weast, Cleveland, 1970, 201.
8. Aufderhaar, H. C., Smith, L. R. and Leslie, W. C., *Metal Handbook, Properties of Pure Metals*, Vol.2, 9th edn. American Society for Metals, Metals Park, Ohio. 1979, pp. 724, 744.
9. Nawa, M., Sekino, T. and Niihara, K., Fabrication and mechanical behaviour of $Al_2O_3$/Mo nanocomposites. *J. Mat. Sci.*, 1994, **29**, 3185–3192.
10. Trusty, P. A. and Yeomans, J. A., The toughening of alumina with iron: effects of iron distribution on fracture toughness. *Journal of the European Ceramic Society*, 17, **1886**, 495–504.
11. Walton, J. D. and Poulos, N. E., Cermets from thermite reactions. *J. Am. Ceram. Soc.*, 1959, **42**, 40–49.
12. Tuan, W. H. and Brook, R. J., The toughening of alumina with nickel inclusions. *Journal of the European Ceramic Society*, 1990, **6**, 31–37.
13. Tuan, W. H., Wu, H. H. and Yang, T. J., The preparation of $Al_2O_3$/Ni composites by a powder coating technique. *J. Mat. Sci.*, 1995, **30**, 855–859.
14. Breval, E., Deng, Z., Chiou, S. and Pantano, C. G., Sol–Gel prepared Ni–alumina composite materials. Part I. Microstructure and mechanical properties. *J. Mat. Sci.*, 1992, **27**, 1464–1468.
15. Loehman, R. E. and Ewsuk, K. G., Synthesis of $Al_2O_3 - Al$ composites by reactive metal penetration. *J. Am. Ceram. Soc.*, 1996, **79**, 27–32.
16. Rödel, J., Prielipp, H., Claussen, N., Sternitzke, M., Alexander, K., Becher, P. F. and Schneibel, J. H., $Ni_3Al/Al_2O_3$ composites with interpenetrating networks. *Scr. Metall. & Mater.*, 1995, **33**, 843–0848.
17. Schicker, S., Garcia, D. E., Bruhn, J., Janssen, R. and Claussen, N., Reaction processing of $Al_2O_3$ containing iron and iron aluminides. *J. Am. Ceram. Soc.*, 1997.
18. Secondi, J. and Yavari, R., Ceramic and metal–ceramic nanostructures obtained by reactive ball milling. *J. de Physique IV, Colloque C7*, 1993, **3**, 1287–1292.
19. Matteazzi, P. and Le Caer, G., Synthesis of nanocrystalline alumina–metal composites by room-temperature ball-milling of metal oxides and aluminium. *J. Am. Ceram. Soc.*, 1992, **75**, 2749–2755.
20. Osso, D., Tillement, O., Mocellin, A., Le Caer, G., Babushkin, O. and Lindback, T., Mechanical–thermal synthesis of $Al_2O_3$–Cr composite powders. *Journal of the European Ceramic Society*, 1995, **15**, 1207–1212.
21. Wang, L. L., Munir, Z. A. and Maximov, Y. M., Review: thermite reactions: their utilization in the synthesis, processing materials. *J. Mat. Sci.*, 1993, **28**, 3693–3708.
22. Chernenko, E. V., Afanaseva, L. F., Lebedeva, V. A. and Rozenband, V. I., Combust. Explos. Schock Waves. *(English Translation)*, 1988, **24**, 639.
23. Osso, D., Elaboration de nanocomposites alumine–métal (Fe,Cr,Ni) par mécanosynthèse, Ph.D. thesis, INPL Nancy, France, 1995.
24. Thiessen, K. P., On the origin of increased activity in mechanochemistry of solids. *J. de Chimie Physique*, 1986, **83**, 717–724.
25. Gleiter, H., Nanocrystalline materials. *Progress in Mat. Sci.*, 1989, **33**, 223–315.
26. Williamson, G. and Hall, W. H., X-ray line broadening from filed aluminium and wolfram. *Acta Met.*, 1953, **1**, 22–31.
27. Chantikul, P., Anstis, G. R., Lawn, B. R. and Marshall, D. B., A critical evaluation of indentation techniques for measuring fracture toughness: II. Strength method. *J. Am. Ceram. Soc.*, 1981, **64**, 539–543.
28. Lux, F., Review: Models proposed to explain the electrical conductivity of mixtures made of conductive and insulating materials. *J. Mat. Sci.*, 1993, **28**, 285–301.

29. Lee, S. I., Noh, T. W., Chen, X. D. and Gaines, J. R., Experimental observation of nonuniversal behavior of the conductivity exponent for three-dimensional continuum percolation systems. *Phys. Rev. B*, 1986, **34**, 6719–6724.
30. Shinozaki, K., Ishkura, Y., Vematsu, K., Mizutami, N. and Kato, M., Vickers micro-hardness of solid solution in the system $Cr_2O_3$–$Al_2O_3$. *J. Mat. Sci.*, 1980, **15**, 1314–1316.
31. Munir, Z. A., Analysis of the origin of porosity in combustion-synthesized materials. *J. of Materials Synthesis and Processing*, 1993, **1**(6), 387–394.
32. Wang, K. Y., Shen, T. D., Qhan, M. X. and Wang, J. T., Self-sustaining reaction during mechanical alloying of $Ni_{60}Ti_{40}$ in oxygen atmosphere. *Scr. Metall. Mater.*, 1992, **26**, 933–397.
33. Park, Y. J. and Kim, J. H. P. *J. Korean Inst. Met. Mater.*, 1978, **16**, 463.
34. Dunmead, S. D., Munir, Z. A., Holt, J. B. and Kingman, D. D., Simultaneous synthesis and densification of TiC/Ni–Al composites. *J. Mat. Sci.*, 1991, **26**, 2410–2416.